Article

A Robust Assessment Model of the Solar Electrical-Thermal Energy Comprehensive Accommodation Capability in a District Integrated Energy System

Wei Wei [1], Haoyue Jia [1,*], Yunfei Mu [1], Jianzhong Wu [2] and Hongjie Jia [1]

[1] Key Laboratory of Smart Grid of Ministry of Education, Tianjin University, Tianjin 300072, China; weiw@tju.edu.cn (W.W.); yunfeimu@tju.edu.cn (Y.M.); hjjia@tju.edu.cn (H.J.)

[2] School of Engineering, Cardiff University, Cardiff CF24 3AA, UK; wuj5@cardiff.ac.uk

* Correspondence: 3012203247@tju.edu.cn; Tel.: +86-182-2233-3907

check for updates

Abstract: As effective utilization of solar resources is a significant way to address the imbalance between energy supply and demand. Therefore, reasonably assessing the accommodation capability of solar energy is important. A two-stage robust evaluation model is proposed for the solar electricity-thermal energy comprehensive accommodation capability in a district integrated energy system. The accommodation capability index is constructed based on the second law of thermodynamics. A robust optimization model was adopted to deal with the uncertainty of solar irradiance. In the solution procedure, the non-convex non-linear power flow model is transformed into a second-order cone model to effectively fit the proposed two-stage robust evaluation model. Finally, a case study verifies the effectiveness of the proposed model and the solution method. The influence of irradiance fluctuation range, gas boiler, and energy storage is discussed in detail.

Keywords: integrated energy system; solar energy; electrical-thermal energy comprehensive accommodation; robust optimization

1. Introduction

Renewable energy (e.g., solar) can effectively solve the problem of air pollution caused by fossil fuels, help adjust the energy structure, and maintain energy security because of its cleanness, sustainability, and limitless usage. Therefore, the development of renewable energy can be of great significance to our socioeconomic life. However, renewable energy sources have the characteristics of randomness and intermittence. Large-scale usage of renewable energy will bring new challenges to the operation of energy systems [1]. Reasonably assessing the accommodation capability of renewable energy is an important measure to face these challenges.

An integrated energy system (IES) that integrates generation, transmission, conversion, and consumption of multiple types of energy can take the full advantage of the complementary and comprehensive effects of different energy carriers, which is an important way to improve the accommodation of renewable energy. So far, many references have carried out research on renewable energy accommodation based on the comprehensive utilization of energy. Reference [2] studied the influence of combined heat and power (CHP) unit on wind power accommodation. In Reference [3], wind power accommodation by electric boiler was studied and the feasibility of thermal supply, by wind power, was demonstrated. In Reference [4,5], the effects of thermal energy storage (TES) and heat pump (HP) technology on the Danish wind power accommodation capability were studied. Reference [6] studied the impact of optimal operation of TES, in a heating network, on increasing

wind power accommodation. Reference [7] studied the effect of the electrical-thermal coordinated operation mode on the benefits of wind power accommodation. Reference [8] studied the renewable energy accommodation considering thermal storage capacity of buildings and temperature range that people could tolerate. Reference [9] studied the comprehensive demand response ability of a small domestic energy supply system consisting of CHP units, electrical boiler, and photovoltaic (PV) power generation equipment, and confirmed that the flexible demand response technology could effectively cope with the uncertainty of PV output. Reference [10] proposed that an IES system with multi-zone heat-supply network interaction could improve the solar energy utilization. But it focused on the economy of planning, not the accommodation capability of solar energy in an IES. Reference [11] evaluated the accommodation capacity of photovoltaic equipment using random scenario simulation method. Reference [12] assessed the capability of wind power accommodation, considering day-ahead wind power forecasting, and sought an envelope of wind power accommodation. In Reference [13], the random generation simulation and continuous load curves, were used to study the wind power accommodation assessment in the heating season.

The above studies mainly focus on the consumption of renewable energy in the form of electricity, while other energy systems are seen as a supplementation. With the enhancement of people's awareness of environmental protection, the combination of district heating and renewable energy sources have attracted much attention [14]. Reference [15] has studied the feasibility of biomass district heating (BDH) system, which shows that BDH has good economic benefits and can reduce carbon emissions. Reference [16] summarized the solar district heating (SDH) technology and discussed the economic feasibility of centralized SDH, and distributed SDH, respectively. Reference [17] shows that negative residual power from wind farms, which could be used in district heating system through power-to-heat infrastructures. In the actual operation of an IES, electricity and heat mutually influence each other, and the consumption of renewable energy, in the form of electricity or thermal energy, may be affected by the operation of electrical-thermal coupling equipment, such as a combined heat and power (CHP) unit. Solar collector (SC) technology is also a mature technology of solar energy utilization. Comprehensive solar utilization, in the form of electricity and thermal, together can make full use of the potential of power grid and district heating network, which is helpful in improving the overall solar energy accommodation.

In the study of solar electricity-thermal energy comprehensive accommodation, two issues need to be seriously considered. The first issue is that the value of electrical and thermal energy is different, and no unified evaluation index has been established. At present, two main methods can be used to evaluate the energy value [18]. The first method treats heat and electricity as equivalent, based on the first law of thermodynamics. The second method use exergy to reflect the ability of energy based on the second law of thermodynamics [19–21]. In order to distinguish the value of different energy, the second law of thermodynamics is adopted for evaluating the energy value in this study. The second issue is how to deal with the uncertainty of solar energy. Some solutions have been developed, such as stochastic programming, chance-constrained programming, and robust optimization, which are available for solving solar energy output volatility [22]. The former two methods focus on the influence of the distribution of uncertain variables, which is more suitable for solving cost-benefit problems [23,24]. Robust optimization focuses on the "worst" scenario, which makes the evaluation results relatively conservative, and is more suitable for the evaluation of indicators related to system security [25].

This paper focuses on the electrical-thermal comprehensive utilization of solar energy. A two-stage robust model for evaluating solar energy accommodation, in district IESs, is proposed, and the electrical-heating network constraints and the uncertainty of solar energy is fully considered. The energy value is evaluated based on the second law of thermodynamics. Then, the second-order cone optimization method is used to make the power flow model of the distribution network convex, which enables the optimization problem to be effectively solved. Finally, the validity of the model is verified by a case study.

2. District Integrated Energy System Model

The district IES is one of the typical application forms of an IES, which consists of three parts: Energy supply, energy conversion, transmission and energy consumption. The energy supply part mainly includes an upstream power grid, solar energy, wind power, and natural gas. The energy conversion and transmission parts mainly include distributed generations, heating units, energy storage device, a distribution power network, and a district heating network. The energy consumption part includes the electricity load and thermal load. Figure 1 shows a typical structure of a district IES.
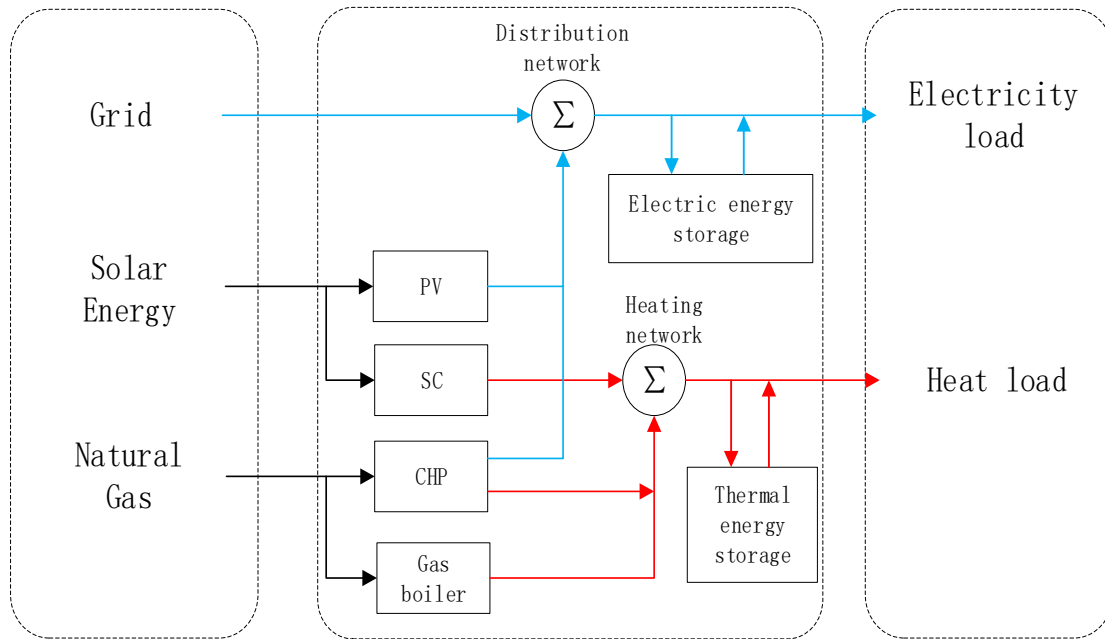
Figure 1. Schematic diagram of a district integrated energy system.

2.1. The Equipment Model

(1) The Photovoltaic Model

Photovoltaic power generation technology converts solar energy into electrical energy, mainly including a photovoltaic array, an inverter, a filter boost circuit, and related control devices. The general model of PV generation is as follow:

$$P_{i,pv} = A_{i,pv} I_i \eta_{pv} = \frac{I_i}{I_s} C_{i,pv} \tag{1}$$

where $P_{i,pv}$ represents the actual output power of the PV power generation system at node i, MW; $A_{i,pv}$ is the installation area of the PV system at node i, m^2; I_i represents the actual irradiance intensity of the system at node i, MW/m^2; η_{pv} represents the PV conversion efficiency of the PV system; $C_{i,pv}$ represents the PV capacity installed at node i, MW, with its value equal to the actual PV output under standard irradiance intensity; and I_S represents the irradiance intensity under standard conditions (temperature of 25 °C and atmospheric quality of AM1.5), which is 1×10^{-3} MW/m^2 in this paper.

(2) The Solar Collector Model

A solar collector can collect the heat of solar radiation and exchange thermal energy with the heat exchanger to heat the cold water in the heating system. The general model of SC is as follow:

$$H_{i,col} = A_{i,col} I_i \eta_{col} = \frac{I_i}{I_s} C_{i,col} \tag{2}$$

where $H_{i,col}$ represents the thermal output of the SC at node i, MW; η_{col} represents the efficiency of the SC; $A_{i,col}$ is the installation area of the SC at node i, m^2; and $C_{i,col}$ represents the SC capacity installed at node i, MW, with its value equal to the SC output under standard irradiance intensity.

(3)　Installation Area Constraints of Solar Panels

The solar energy reaching the earth's surface is received by PV power panels and SCs. Constrained by the site, the total area of solar power panels and SCs that can be installed in the system is limited, so the solar power that can be received is also limited. That is:

$$0 \le A_{i,pv} + A_{i,col} \le \overline{A_i} \tag{3}$$

where $\overline{A_i}$ is the maximum area of solar energy equipment installed at node *i.*

(4)　The CHP Unit Model

CHP units generate electricity by steam turbine, as well as supplying thermal energy to thermal users through steam after power generation. It is one of the key components of the electrical-thermal integrated energy system and the main source of heat supply for civil and commercial use in China. CHP units can be divided into back-pressure units and extraction condensing units. Their operation characteristics can be described by a series of linear inequality constraints [7], and the model is as follows:

$$\begin{cases} \alpha_1 P_{i,chp} + \beta_1 H_{i,chp} \le \gamma_1 \\ \alpha_2 P_{i,chp} + \beta_2 H_{i,chp} \le \gamma_2 \\ \cdots \\ \alpha_{N_i} P_{i,chp} + \beta_{N_i} H_{i,chp} \le \gamma_N \end{cases} \tag{4}$$

where $\alpha_1 \sim \alpha_{N_i}$, $\beta_1 \sim \beta_{N_i}$ and $\gamma_1 \sim \gamma_{N_i}$ are the coefficients of the inequality constraints on the operating range of CHP units at node i; the subscript N_i is the number of inequality constraints on the operating range of CHP units at node i; $P_{i,chp}$ is the power output of the CHP unit at node i, MW; and $H_{i,chp}$ is the thermal output of the CHP unit at node i, MW.

(5)　Output Constraints of Gas Boilers

Gas boilers use natural gas as fuel to convert the chemical energy of fuel into thermal energy, which is characterized by energy saving, environmental protection, and high economic efficiency. The output constraint of gas boiler is as follow:

$$0 \le H_{i,gb} \le \overline{H}_{i,gb} \tag{5}$$

where $H_{i,gb}$ represents the thermal output of the gas boiler at node i, MW; $\overline{H}_{i,gb}$ is the maximum thermal output of the gas boiler at node i, MW.

(6)　Energy Storage Device Model

Energy storage technology is one of the most important parts in the study of renewable energy consumption and utilization in integrated energy systems. The energy storage device includes an electrical energy storage device and the thermal energy storage device, which are used for the storage of electrical energy, and thermal energy, respectively. The model is as follows:

$$S_{i,t+1} = S_{i,t} + \Delta t P_{es,i,t} \tag{6}$$

$$\begin{cases} 0 \le S_{i,t} \le S_i^{\max} \\ P_{dis}^{\max} \le P_{es,i,t} \le P_{cha}^{\max} \\ S_{i,1} = S_{i,t+24} \end{cases} \tag{7}$$

$$TS_{i,t+1} = TS_{i,t} + \Delta t H_{ts,i,t} \tag{8}$$

$$\begin{cases} 0 \le TS_{i,t} \le TS_i^{\max} \\ H_{dis}^{\max} \le H_{ts,i,t} \le H_{cha}^{\max} \\ TS_{i,1} = TS_{i,t+24} \end{cases} \tag{9}$$

where $S_{i,t}$ and $TS_{i,t}$ are the storage states of the electrical and thermal storage devices. $P_{es,i,t}$ and $H_{ts,i,t}$ are the charging and discharging power/heat at time t. $P_{dis}^{\max}$ is the maximum discharging power of the electrical storage device, and it is a negative number. $P_{cha}^{\max}$ is the maximum charging power of the electrical storage device. $H_{dis}^{\max}$ is the maximum discharging heat of the thermal storage device, and it is a negative number. $H_{cha}^{\max}$ is the maximum charging heat of the thermal storage device. In addition, the storage states at the initial and ending times should be the same.

2.2. The Electrical Network Model

In this paper, DistFlow model is used to construct electrical distribution network. And it is converted into a second-order model to make the problem easy to solve.

2.2.1. DistFlow Model

In a district IES, the power network is usually the distribution network running in a radial manner [26]. DistFlow is a widely accepted power flow model suitable for the radial structure of the most powerful distribution systems [27]. It is computationally superior to the Newton-Raphson and Gauss-Seidel methods because it does not require the admittance matrix calculation to optimize the distribution system [28].

$$\sum_{i \in \delta(j)} (P_{ij} - r_{ij} I_{ij}^2) + P_j = \sum_{k \in \xi(j)} P_{jk} \tag{10}$$

$$\sum_{i \in \delta(j)} (Q_{ij} - x_{ij} I_{ij}^2) + Q_j = \sum_{k \in \xi(j)} Q_{jk} \tag{11}$$

$$U_j^2 = U_i^2 - 2(r_{ij} P_{ij} + x_{ij} Q_{ij}) + (r_{ij}^2 + x_{ij}^2) I_{ij}^2 \tag{12}$$

$$U_i^2 I_{ij}^2 = P_{ij}^2 + Q_{ij}^2 \tag{13}$$

$$P_i = P_{i,chp} + P_{i,pv} + P_{grid} - P_{i,load} - P_{i,es} \tag{14}$$

$$Q_i = Q_{i,chp} + Q_{grid} - Q_{i,load} - Q_{i,ts} \tag{15}$$

where $\delta(j)$ represents the set of head nodes of the branches whose end node is j; $\xi(j)$ represents the set of end nodes of the branches whose head node is j; P_{ij} and Q_{ij} are the active and reactive power from node i to node j, respectively; P_i and Q_i are the active, and reactive injected power of node i, respectively; r_{ij} and x_{ij} are the resistance, and reactance of branch ij, respectively; I_{ij} is the current amplitude of branch ij; U_i is the voltage amplitude of node i; P_{grid} and Q_{grid} represent the active and reactive power injected by the large power grid, only included in the equation at the equilibrium node; and $P_{i,load}$ and $Q_{i,load}$ represent the active load and reactive load at node i.

2.2.2. Distflow Second-Order Cone Model

The above power flow model is a non-convex non-linear model. Solving a robust optimization model with min-max form including non-linear constraints is a NP-hard problem [29]. To overcome the NP-hard problem, this paper converts the Distflow model into a second-order cone model by adopting the method proposed in Reference [30]. First, define new variables $u_i = U_i^2$ and $i_{ij} = I_{ij}^2$. Second, substitute these two variables into the original Distflow model. The result is as follows:

$$\sum_{i:i \to j} (P_{ij} - r_{ij} i_{ij}) + P_j = \sum_{k:j \to k} P_{jk} \tag{16}$$

$$\sum_{i:i\to j}\left(Q_{ij}-x_{ij}i_{ij}\right)+Q_j=\sum_{k:j\to k}Q_{jk} \tag{17}$$

$$u_j=u_i-2\left(r_{ij}P_{ij}+x_{ij}Q_{ij}\right)+\left(r_{ij}^2+x_{ij}^2\right)l_{ij} \tag{18}$$

$$u_ii_{ij}=P_{ij}^2+Q_{ij}^2 \tag{19}$$

Furthermore, the quadratic constraint of the branch apparent power, shown in Equation (13), can be relaxed to the cone constraint:

$$u_ii_{ij}\ge P_{ij}^2+Q_{ij}^2 \tag{20}$$

Equation (20) can be expressed in standard second-order cone form through an equivalent transformation:

$$\left\|\begin{array}{c}2P_{ij}\\2Q_{ij}\\i_{ij}-u_i\end{array}\right\|_2\le i_{ij}+u_i \tag{21}$$

The constraints of the node voltage and branch current can be expressed as:

$$\left(\underline{U}\right)^2\le u_i\le\left(\overline{U}\right)^2 \tag{22}$$

$$0\le i_{ij}\le\left(\overline{I}\right)^2 \tag{23}$$

where $\underline{U}$ and $\overline{U}$ are the upper and lower limits of the node voltage; $\overline{I}$ is the maximum allowable current of the branch.

The Distflow power flow equations have thus been converted into a convex model with only a few second-order cone constraints.

2.3. The District Heating Network Model

To facilitate the establishment of a robust model, this paper adopts the linear heating network energy flow model proposed in Reference [31].

$$\left\{\begin{array}{ll}H_{s,i}+\sum\limits_{j\in I}H'_{ij}=0\\H'_{ij}=-\left(H'_{ji}-\Delta H'_{ji}\right)&\text{if }H'_{ij}>0\\H'^{\min}_{ij}\le H'_{ij}\le H'^{\max}_{ij}&\text{if }H'_{ij}>0\end{array}\right. \tag{24}$$

$$\left\{\begin{array}{l}\Delta H'=2\pi\frac{T_s-T_a}{\sum R}l_{ij}\\H'^{\min}_{ij}=2\pi\frac{T_s-T_a}{\sum R}l_{ij}\\H'^{\max}_{ij}=c_p\rho v_{ij}^{\max}S_{ij}(T_s-T_r)\\H_{s,i}=H_{i,chp}+H_{i,col}-H_{i,load}\end{array}\right. \tag{25}$$

where $H_{s,i}$ is the thermal power injected into node i, MW. H'_{ij} is the available thermal power contained in the thermal medium flowing into node i of the water supply pipeline $i-j$. When the thermal medium flows out of node i, H'_{ij} is negative; otherwise, it is positive, MW. $\Delta H'$ is the loss of thermal power in the pipeline, $\Delta H'_{ij}=-\Delta H'_{ji}$, MW. $H'^{\min}_{ij}$, $H'^{\max}_{ij}$ are the minimum and maximum thermal power that can be transmitted in the pipe, MW. $\sum R$ is the thermal resistance of the pipe per kilometer from the thermal medium to the surrounding medium, $km\cdot{}^\circ C/MW$. $v_{ij}^{\max}$ is the maximum allowable velocity in the pipe, m/s. S_{ij} is the cross-sectional area of the pipe, m^2. T_s is the water supply temperature $^\circ C$. T_r is the water return temperature, $^\circ C$. T_a is the environment temperature, T_r. l_{ij} is the length of the pipeline, km. c_p is the specific heat capacity of the fluid, $MJ/(kg\cdot{}^\circ C)$. ρ is the fluid density, kg/m^3.

According to Reference [31], the loss in the district heating network is assumed to be basically unchanged under different operating conditions, with a fixed T_s, and it is not considered an optimization target.

3. The Robust Assessment Model for Solar Energy Accommodation

With the proposed two-stage robust model, the maximum solar energy accommodation capacity, under the worst scenario, is found. In this paper, the worst scenario is that the value of irradiance intensity under the amount of solar energy consumed is the smallest.

3.1. The Uncertainty Model of Solar Energy Output

The output of PV and SC systems is affected by the irradiance intensity and has the characteristics of randomness and intermittence. This paper adopts a box uncertainty set to describe the irradiance intensity:

$$U : \left\{ \begin{array}{c} u = \left(\widetilde{I} \right)^{\mathbf{T}} \\ \widetilde{I} \in \left[\hat{I} - \Delta I, \hat{I} + \Delta I \right] \end{array} \right\} \tag{26}$$

where $\widetilde{I}$ represents the actual irradiance intensity; $\hat{I}$ represents the predicted irradiance intensity, which can be obtained from meteorological data; and ΔI is the fluctuation range of irradiance intensity set according to the actual situation, which belongs to the uncertainty set U.

The output model of the PV and SC systems can then be expressed as:

$$P_{i,pv} = A_{i,pv} \widetilde{I}_i \eta_{pv} = \frac{\widetilde{I}_i}{I_s} C_{i,pv} \tag{27}$$

$$H_{i,col} = A_{i,col} \widetilde{I}_i \eta_{col} = \frac{\widetilde{I}_i}{I_s} C_{i,col} \tag{28}$$

The conservativeness and robustness of the model can be adjusted by introducing an uncertainty adjustment budget. Uncertainty budget constraints essentially limit the overall deviation of uncertain variables from the predicted values. Irradiance intensity, at different locations or time, should also meet the following constraints:

$$\sum_k \frac{\left| \widetilde{I}_k - \hat{I}_k \right|}{\Delta I_k} \leq \Gamma \tag{29}$$

where k represents location or time which can be selected according to the study to control the uncertainty of irradiance from the view of space or time. Γ is the uncertainty adjustment budget, indicating how many uncertain variables could reach the boundary. The maximum value of Γ is the total number of uncertain variables. When the maximum value is obtained, all uncertain parameters could reach the boundary. When it is set to 0, the robust model degenerates into a deterministic model.

3.2. The objective Function

The output of PV power generation and SC equipment is used to evaluate the accommodation of solar energy in the IES. Without considering solar energy curtailment, the solar-thermal power accommodation level is proportional to the installation capacity of the corresponding power generation and SC equipment. Regarding the quality of different energy, the value factors of electrical and thermal are used [19]. The value factor of electrical equals 1. Additionally, an increase in the power grid loss is equivalent to an increase in the power load of the system. If only the output of solar equipment is taken as the objective function, then the power grid loss in the result may be too large. To achieve the

combined goal of clean and efficient energy utilization, this paper introduces the network loss term into the objective function, as shown in Equation (30):

$$\min_{x} \left[-\sum \left(C_{i,pv} + \tau C_{i,col} \right) + \max_{u \in U} \min_{y \in \Omega(x,u)} \omega P_{loss} \right] \tag{30}$$

where, τ is the value factor of thermal, $\tau = \left(1 - \frac{T_a}{T_s} \right)$; ω is the weight coefficient of power grid loss. Considering the order of magnitude of both parts, 10~100 is recommended to be taken as the value of ω; P_{loss} is the total power grid loss;i is the node of the electricity and heating systems where solar energy equipment is connected; x, y is the optimization variables; $\Omega(x, u)$ is the feasible region of y when a set of (x, u) is given.

The minimization of the outer layer is the first-stage problem. The objective of the first-stage problem is the maximum installation capacity of solar power generation equipment, with $x = \left(A_{i,pv}, A_{i,col} \right)$ as the optimization variable. The max-min problem of the inner layer is the second-stage problem. The objective is the minimum loss of the power grid under the condition of the worst irradiance intensity, with the uncertainty set of irradiance intensity $u = (\widetilde{I})$ and the second-stage control variable y as the optimization variables, where:

$$y = \left(\begin{array}{c} P_{ij}, Q_{ij}, P_i, Q_i, i, u, H_{i,chp}, \\ P_{i,chp}, P_{i,pv}, P_{grid}, P_{i,es}, Q_{grid}, \\ H_{s,i}, H'_{ij}, H_{i,col}, H_{i,gb}, H_{i,ts} \end{array} \right) \tag{31}$$

3.3. The Constraints

Equations (3)–(9), (14)–(18) and (21)–(29) are the constraints of the robust model.

4. Solution of the Robust Model

In the previous section, a two-stage robust evaluation model of solar energy accommodation is built, which can be solved by the column-and-constraint generation (C&CG) algorithm proposed in Reference [32]. The C&CG algorithm decomposes objective function into a main problem and a subproblem, and the optimal solution of the original problem is obtained by solving them alternately.

For convenience, the model can be written in the following compact form [27]:

$$\min_{x} b^T x + \left\{ \max_{u \in U} \min_{y \in \Omega(x,u)} c^T y \right\} \tag{32}$$

where b is a vector only consisting of values of -1.

The compact form of constraints is shown as follows:

$$\begin{cases} Dy \geq d & \rightarrow \lambda \\ H(x)y = u & \rightarrow \pi \\ \|G_i y\|_2 \leq g_i^T y & \rightarrow \sigma, \mu \\ Fx \geq f \end{cases} \tag{33}$$

where $Dy \geq d$ corresponds to Equations (4)–(9), (14)–(19) and (22)–(25); $H(x)y = u$ corresponds to Equations (27) and (28), with $H(x)$ a coefficient matrix expressed in the form of a function of x; $\|G_i y\|_2 \leq g_i^T y$ corresponds to formula (21); and $Fx \geq f$ corresponds to equation (3). One equality constraint can be rewritten as two inequality constraints, so the compact form above does not include the equality constraint form. λ, π, σ, μ are the dual variables of the corresponding constraints in the second-stage problem. Equation (3) only contains the first-stage variables, so there are no dual variables.

The main problem and the subproblem can be obtained by decomposing Equation (32).

(1) The Main Problem

The main problem of the two-stage robust model has the following form:

$$\min_x b^T x + \eta$$

$$s.t. \quad \begin{cases} \eta \geq c^T y^l \forall l \in O \\ Dy^l \geq d \\ H(x)y^l = u^l \quad l = 1,2,3\cdots \\ \|G_i y^l\|_2 \leq g_i^T y^l \\ Fx \geq f \end{cases} \tag{34}$$

where η is the introduced auxiliary variable; l represents the number of iterations; y^l and u^l represent the new variables and worst case scenarios introduced into the main problem during the lth iteration; and O is a collection of the number of feasible cuts.

In the main problem, x and y^l are the decision variables, and the values of the uncertain parameter are fixed.

(2) The Sub-Problem

The sub-problem of the two-stage robust model has the following form:

$$\max_{u \in U} \min_{y \in \Omega(x,u)} c^T y$$

$$st. \quad \begin{cases} Dy \geq d \\ H(x)y = u \\ \|G_i y\|_2 \leq g_i^T y \end{cases} \tag{35}$$

The sub-problem of the two-stage robust model is a min-max problem. According to the dual theory of linear programming and second-order cone programming, the inner dual maximization problem and the outer maximization problem can be merged. The transformed form is as follows:

$$\max d^T \lambda + u^T \pi$$
$$s.t. \ D^T \lambda + H(x)^T \pi + \sum (G_i^T \sigma_i + g_i \mu_i) = c$$
$$\|\sigma_i\|_2 \leq \mu_i \tag{36}$$
$$\lambda, \mu \geq 0, \pi, \sigma \text{ are free variables}, u \in U$$

where $\lambda, \pi, \mu, \sigma$ are the dual variables introduced for the dual problem.

In the sub-problem, the bilinear term $u^T \pi$ is included, and the related constraints of the dual variables constitute a polyhedral set. According to Reference [27], if there is an optimal solution to the sub-problem, it will be obtained at one extreme of the uncertainty set. For a box uncertainty set, the set of all its extremes can be expressed as:

$$U' \begin{cases} u = \hat{u} + (\theta^+ - \theta^-)\Delta u \\ \theta^+, \theta^- \in \{0,1\} \\ \theta^+ + \theta^- \leq 1 \\ \sum (\theta^+ + \theta^-) = \Gamma \end{cases} \tag{37}$$

where $\hat{u}$ is the predicted value of the uncertain variables, namely, the central value. θ^+, θ^- are 0–1 variables, whose values are, respectively, (0,0), (0,1) or (1,0), meaning that the uncertain variables have the predicted, lower limit and upper limit values, respectively.

Substituting U' into Equation (36) yields:

$$\max d^T\lambda + \widehat{u}^T\pi + \Delta u^T(\theta^+ - \theta^-)\pi$$
$$s.t.\ D^T\lambda + H(x)^T\pi + \sum(G_i^T\sigma + g_i\mu) = c$$
$$\|\sigma_i\|_2 \le \mu_i$$
$$\theta^+, \theta^- \in \{0,1\} \qquad (38)$$
$$\theta^+ + \theta^- \le 1$$
$$\sum(\theta^+ + \theta^-) = \Gamma$$
$$\lambda, \mu \ge 0, \pi, \sigma \text{ are free variables}$$

The last term of the objective function in Equation (38) is still a bilinear term. According to Reference [33], the big M method is adopted for this problem.

$$B_1 = \theta^+\pi \Leftrightarrow \left\{ \begin{array}{l} -M\theta^+ \le B_1 \le M\theta^+ \\ \pi - M(1-\theta^+) \le B_1 \le \pi + M(1-\theta^+) \end{array} \right\}$$
$$B_2 = \theta^-\pi \Leftrightarrow \left\{ \begin{array}{l} -M\theta^- \le B_2 \le M\theta^- \\ \pi - M(1-\theta^-) \le B_2 \le \pi + M(1-\theta^-) \end{array} \right\} \qquad (39)$$

where M is a sufficiently large positive real number. B_1 and B_2 are the introduced auxiliary variables.

Then, Equation (38) can be expressed as:

$$\max d^T\lambda + \widehat{u}^T\pi + \Delta u^T(B_1 - B_2)$$
$$s.t.\ D^T\lambda + H(x)^T\pi + \sum(G_i^T\sigma + g_i\mu) = c$$
$$\|\sigma_i\|_2 \le \mu_i$$
$$-M\theta^+ \le B_1 \le M\theta^+$$
$$\pi - M(1-\theta^+) \le B_1 \le \pi + M(1-\theta^+)$$
$$-M\theta^- \le B_2 \le M\theta^- \qquad (40)$$
$$\pi - M(1-\theta^-) \le B_2 \le \pi + M(1-\theta^-)$$
$$\theta^+, \theta^- \in \{0,1\}$$
$$\theta^+ + \theta^- \le 1$$
$$\sum(\theta^+ + \theta^-) = \Gamma$$
$$\lambda, \mu \ge 0, \pi, \sigma \text{ are free variables}$$

Formula (40) is a mixed integer second-order cone programming model, which can be solved by the commercial mathematical software using C&CG algorithm.

5. Case Studies and Results

In this paper, the case system in Reference [34] is appropriately modified. The system structure diagram, as shown in Figure 2, includes a 9-node power distribution network and a 32-node district heating network. The network parameters are shown in Reference [34]. The system includes three comprehensive energy stations, all of which are equipped with back-pressure cogeneration (CHP) units and gas boilers (GBs). The back-pressure CHP units in each energy station have a heat-to-power ratio of 1.3, which means that the CHP unit will generate 1 W of electrical power and 1.3 W of heat power at the same time. The maximum output power of CHP is 0.5 MW. The maximum thermal output power of each gas-fired boiler is 0.5 MW. Additionally, the energy station can be equipped with PV power generation equipment (PV) and SCs. The maximum available area for installation of solar energy devices at each energy station is 7500 m^2. The PV energy conversion efficiency is 17.5%, and the SC energy conversion efficiency is 50%.
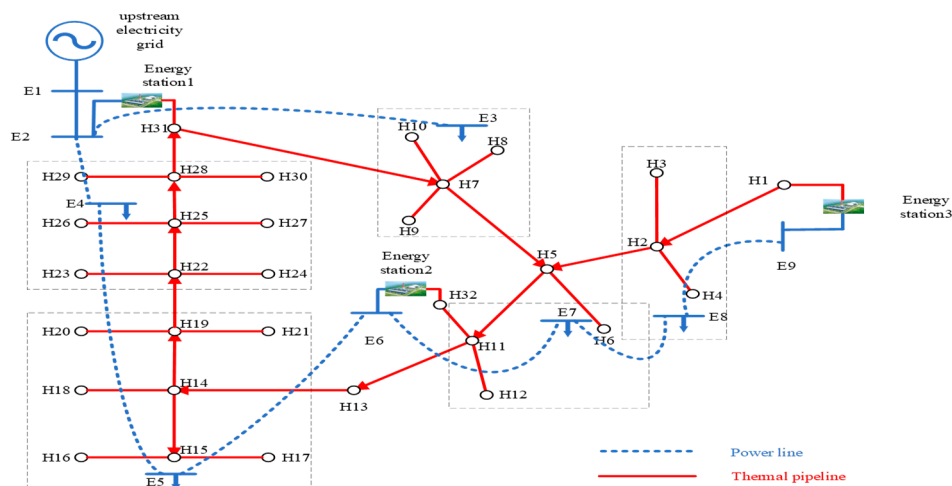
Figure 2. The structure of the case system.

In this paper, the solar energy accommodation capability in a single period is first studied to show the influence of electrical-thermal energy comprehensive accommodation and solar energy uncertainty. Then, the solar energy accommodation capability of 24-h periods is studied to show the effect of energy storage devices.

5.1. Analysis of the Single-Period Case

In the single-period case, the predicted value of irradiance intensity is taken as 566 W/m^2, and power cannot be sent back to the upstream power grid. The load of each node of the system is shown in Appendix A. The base apparent power is 1 MVA and base voltage is 11 kV. The allowable range of the node voltage is 0.9–1.1 per unit (p. u.), and the maximum allowable branch current is 200 A. The maximum allowable flow rate of water in the district heating network pipelines is 2 m/s. The supply temperature of SC and CHP is 90 °C temperature. And the supply temperature of load is 40 °C. Environment temperature is 0 °C. Energy storage equipment is not considered in the single-period case.

Based on the above data, six scenarios are set as follows:

Case 1.1: Deterministic model, only PV devices are considered.
Case 1.2: Deterministic model, both PV and SC devices are considered.
Case 1.3: Robust model, both PV and SC devices are considered; the fluctuation of the irradiance intensity is 5%.
Case 1.4: Robust model, both PV and SC devices are considered; the fluctuation of the irradiance intensity is 10%.
Case 1.5: Robust model, both PV and SC devices are considered; the fluctuation of the irradiance intensity is 15%.
Case 1.6: Robust model, both PV and SC devices are considered; the fluctuation of the irradiance intensity is 20%.

(1) Analysis of Solar Energy Utilization Forms

The accommodation capabilities in Cases 1.1 and 1.2 are shown in Table 1.

Table 1. Accommodation capacity comparison for Cases 1.1 and 1.2.

	Total PV Capacity/MW	Total SC Capacity/MW
Case 1.1	1.759	0
Case 1.2	2.827	3.172

Based on the comparison of Cases 1.1 and 1.2, the utilization of PV power generation and SC equipment together can directly accommodate more 3.172 MW of solar thermal power. Additionally, this system can also accommodate more PV power of 1.068 MW. This result mainly occurs because the SC can reduce the CHP unit's thermal output and therefore reduce the CHP unit's electrical output, which provides more accommodation space for PVs.

(2)   Analysis of the Influence of the Fluctuation Range

The accommodation capability comparison of Cases 1.2 to 1.6 is shown in Figure 3.
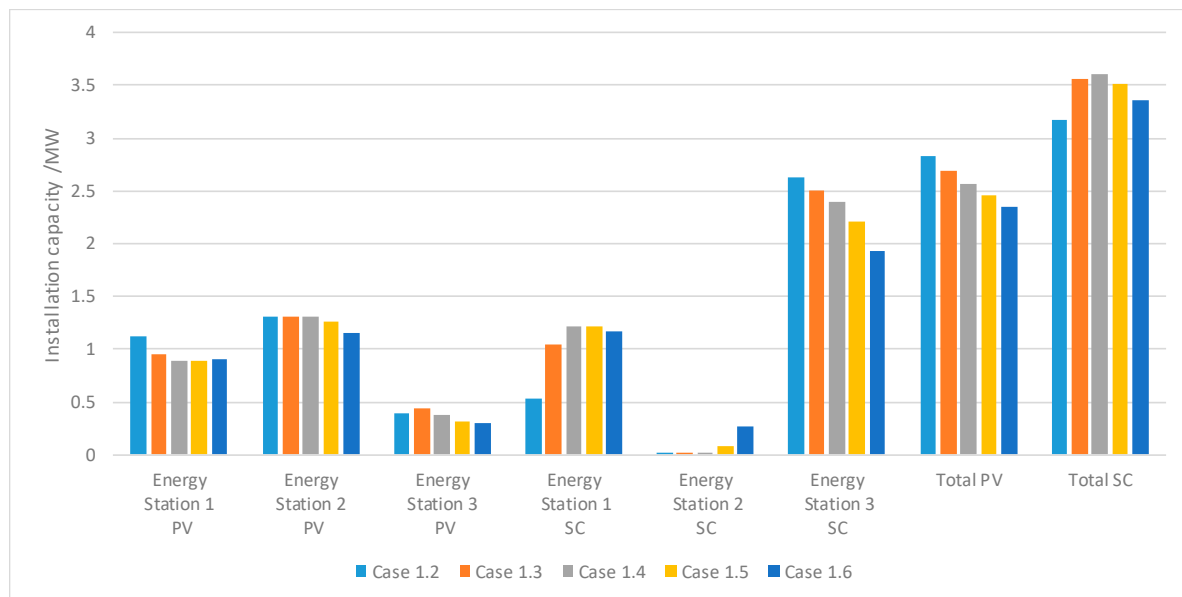
Figure 3. Accommodation capacity comparison of Cases 1.2 to 1.6.

As shown in Figure 3, as the fluctuation range of the solar irradiance intensity increases, the total PV installation capacity presents a monotonic declining trend, while the total accommodated SC capacity first increases and then decreases. By analyzing the case results, the main reason for this phenomenon is that the constraints that restrict the installation capacity of solar energy devices change under different irradiance intensity fluctuation ranges. Figure 4 shows the change process of the accommodated capacity under different irradiance fluctuation ranges.

For the convenience of analysis, the influence of the energy network on the results is not shown in the Figure 4. At this time, the main factors restricting the PV/SC installation capacity include, the maximum installation area of the energy station, and the thermal and electrical loads of the system. When the load is given, the installation area of the solar equipment is inversely proportional to the solar irradiance intensity. The upper bound of the fluctuation range of the irradiance intensity is the main factor limiting solar energy accommodation under sufficient energy supply. The wider the fluctuation range of the irradiance intensity, the higher the fluctuation upper bound is, and the lower maximum accommodation capability.

This paper adopts the second law of thermodynamics to evaluate the thermal and electrical values. In the case of the same installation space, the value of PV is higher than the value of SC, since the energy value factor of PV is much greater than SC. The optimal installation solution is always obtained on the line of the maximum PV installation area constraints under the worst irradiance scenario. In the deterministic model, the irradiance intensity adopts the predicted value, and the optimal installation solution is point A, as shown in Figure 4. The effective constraints of the maximum accommodation capability are the allowable installation area constraints at the energy station and thermal output constraints of the PV under the worst irradiance scenario. The SC installation capacity cannot reach the maximum installation area constrained in the SC thermal output (shown as point A′ in Figure 4). In

Case 1.3, the maximum PV installation area decreases with slight fluctuations of the irradiance intensity. The constraints that affect the maximum accommodation capability are still the allowable installation area constraints and electrical output constraints of the PV, under the worst irradiance scenario. The maximum accommodation capability is shown as point B in Figure 4. Due to the decrease in the PV installation area (the upper limit of the irradiance intensity increases), more space can be provided for the installation of SCs, resulting in an increase of the installation area of SCs. However, due to the limitation of the maximum allowable installation area, the optimal programming scheme at B′ is still not available. When the irradiance intensity uncertainty is further increased, the allowable installation area of the site is no longer an effective constraint, and the PV and SC installation area will decrease with the increase of the fluctuation range, shown as point C in Figure 4.
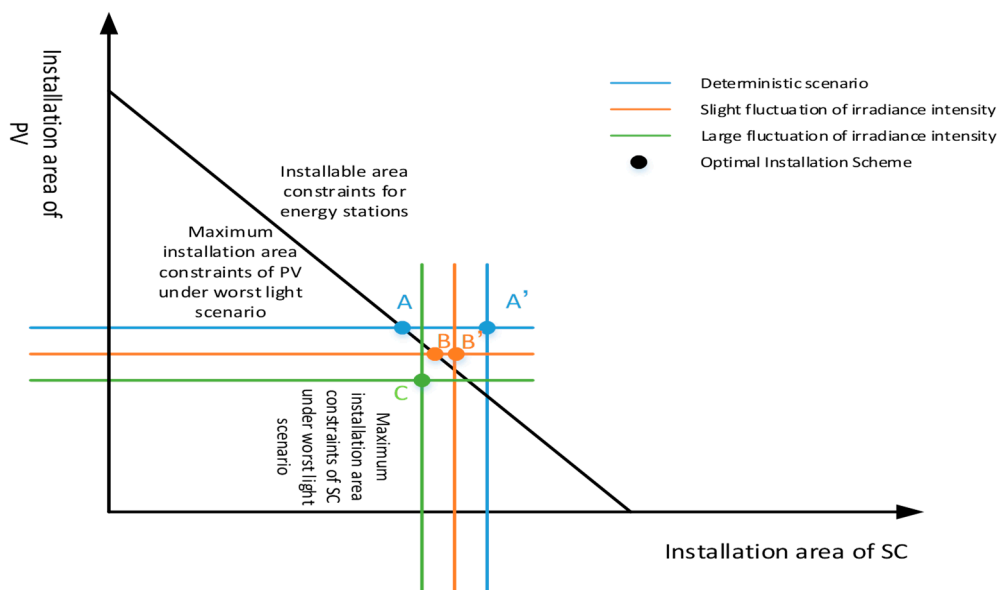

Figure 4. Analysis of the accommodation capacity under different irradiance fluctuation ranges.

(3)   Impact Analysis of Electrical Network Loss

The configuration of solar energy equipment for each energy station is influenced by many factors, such as energy network constraints, load level constraints, and electrical network loss. To reduce the electrical network loss, the local load should be locally supplied as much as possible. As shown in Figure 3, energy stations 1 and 2 are equipped with a large amount of PV power because the power load is mostly concentrated near energy stations 1 and 2, where the installation of PVs can more greatly reduce power grid loss. The factors impact each energy station configuration to a different degree, so that the trend of installation capacity of each energy station, is different.

5.2. Analysis of the 24-h Period Cases

The 24-h case system is the same as the single-period case. Typical irradiance intensity data are extracted from Reference [35], the irradiance intensity fluctuation range is 10%, and the typical load curve is taken from Reference [36]. The maximum thermal load is 1.205 MW, and the maximum electrical load is 1.367 MW, as shown in Figure 5. The equipment that can be installed at each energy station includes CHP units, PV power generation equipment, solar heat collection equipment, GBs, and energy storage equipment. The energy system in the district is not permitted to transmit power to the upstream grid. In order to better illustrate the influence of energy storage equipment, Case 2 does not consider the constraints of allowable area of energy stations.
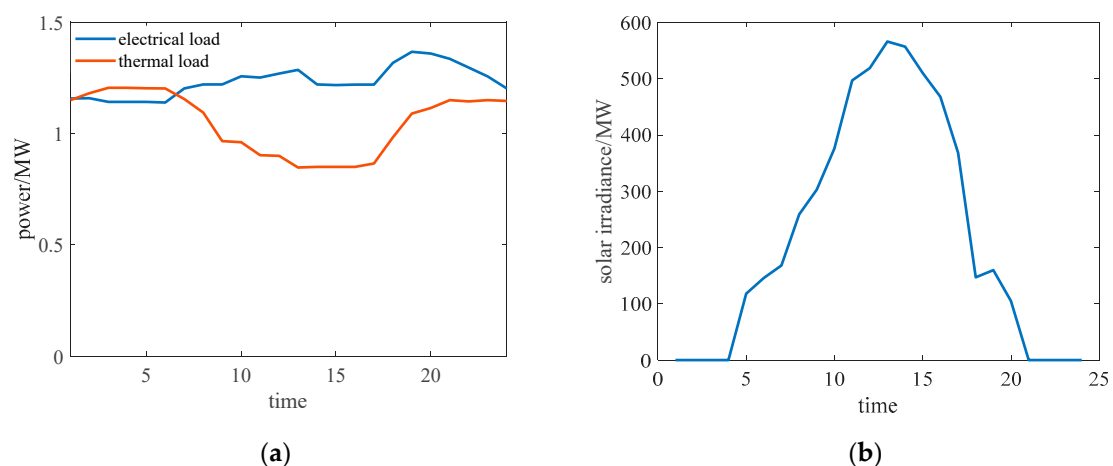
Figure 5. Data for the 24-h period cases. (**a**) Loads of the cases; (**b**) predicted irradiance intensity.

5.2.1. Energy Storage Impact Analysis

The case settings are as follows:

Case 2.1: The system only contains CHP units, PVs and SCs, and the insufficient power is supplied by the upstream grid.

Case 2.2: On the basis of Case 2.1, each of the three energy stations is equipped with a GB with a maximum power of 0.2 MW.

Case 2.3: On the basis of Case 2.1, each of the three energy stations is equipped with electrical energy storage equipment with maximum charge and discharge power of 0.1 MW and a capacity of 0.3 MWh.

Case 2.4: On the basis of Case 2.1, each of the three energy stations are equipped with heat storage equipment with a maximum storage and discharge thermal power of 0.1 MW and a capacity of 0.3 MWh.

Case 2.5: On the basis of Case 2.1, each of the three energy stations are equipped with electrical energy storage equipment, with a maximum charge and discharge power of 0.1 MW and a capacity of 0.3 MWh and heat storage equipment with a maximum charge and discharge thermal power of 0.1 MW and a capacity of 0.3 MWh.

The robust optimization algorithm is used to calculate the PV and SC configuration schemes in achieving the maximum solar energy consumption in the five cases above. The maximum PV and SC installation capacity in each case, as well as the solar electricity and thermal energy accommodation, is shown in Table 2.

Table 2. Configuration results.

	Total PV Capacity/MW	Total SC Capacity/MW	Solar Electricity Accommodation/MW·h [1]	Solar Thermal Energy Accommodation/MW·h [2]
CASE 2.1	1.949	1.556	9.517	7.601
CASE 2.2	1.991	1.556	9.724	7.601
CASE 2.3	2.287	1.556	11.169	7.601
CASE 2.4	1.991	1.992	9.724	9.727
CASE 2.5	2.439	1.992	11.913	9.727

[1,2] Footer: Solar electricity and thermal energy accommodation is calculated under deterministic scenario.

Based on the analysis of the configuration results, the actual PV and SC output power was found to be proportional to the irradiance intensity and installation capacity, regardless of the solar energy curtailment. The PV and SC output power cannot exceed the electrical load and thermal load at the

same time. As the installation capacity increases, the output curves of the PVs and SC will increase proportionally, until the output curves intersect the load curve. The PV and SC maximum capacity at this time corresponds to the maximum solar electric/thermal energy accommodation.

To more clearly explain the reasons for different solar energy accommodation in different cases, the following maximum irradiance intensity scenarios of the five cases are specifically described.

(1) In Case 2.1, the source of the heat energy is only the CHP unit and the SC. The installation capacity of the SC is determined by the thermal load (the load curves in the figure contain power and district heating network losses). As shown in Figure 1, when the SC installation capacity is 1.556 MW, the SC thermal output at 13:00 intersects with the load curve where the SC capacity corresponds to the maximum solar thermal accommodation. When the SC thermal output is determined, the thermal output of the CHP unit is strictly equal to the difference between the thermal load and the SC thermal output, restricted by the thermal load balance. At the same time, the power output of the CHP unit is also determined by the thermal-electrical coupling characteristics of the back-pressure CHP unit. Considering that the system does not permit power transmission to the upstream grid, when the PV installation capacity reaches 1.949 MW, the sum of the output power of the PVs and CHP unit is exactly equal to the power load of the system at 14:00, where the PV capacity corresponds to the maximum solar electricity accommodation. The electrical and thermal power output of Case 2.1 is shown in Figure 6.
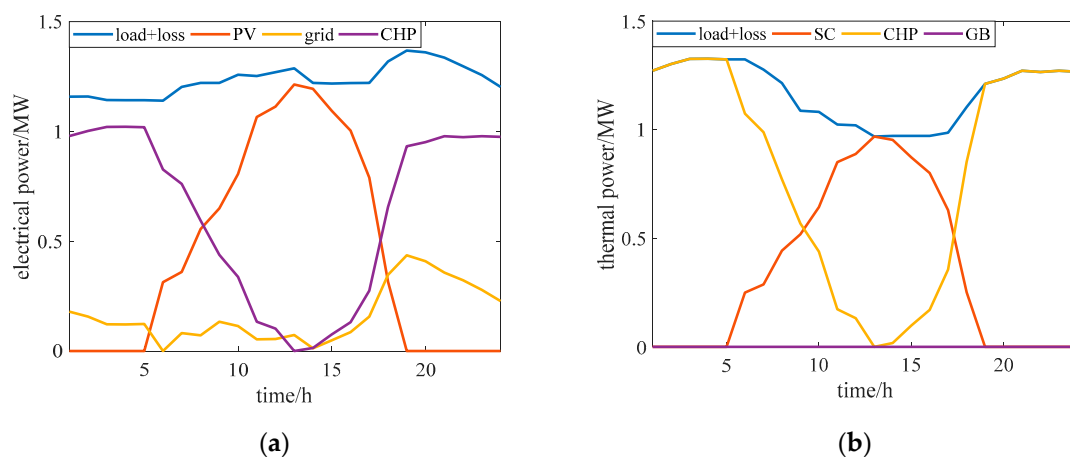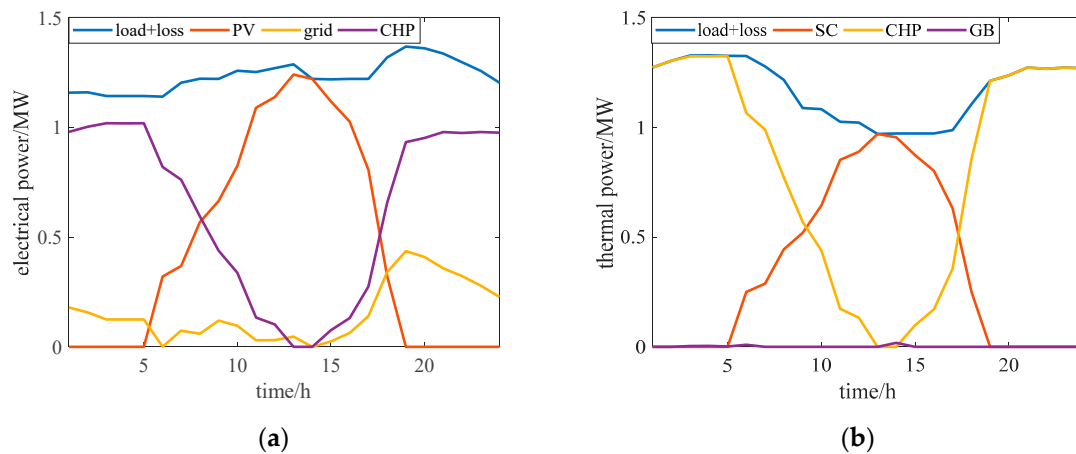

Figure 6. (**a**) Electrical power output in Case 2.1; (**b**) thermal power output in Case 2.1.

(2) In Case 2.2, a GB with a capacity of 0.2 MW is installed. During the period from 13:00 to 14:00, the GB provides part of the thermal power output such that the CHP unit maintains a state of zero output, providing extra space for solar electricity accommodation. The PV installation capacity increases from 1.949 MW in Case 2.1 to 1.991 MW. Since the SC installation capacity is mainly limited by the thermal load, the amount of solar thermal accommodation is relatively unchanged compared with Case 2.1. The electrical and thermal power output of Case 2.2 is shown in Figure 7.

Figure 7. (**a**) Electrical power output in Case 2.2; (**b**) thermal power output in Case 2.2.

(3) In Figure 8, the positive power output of the storage device represents discharge, and negative output represents charge. In Case 2.3, the installed electrical energy storage equipment can be charged from 10:00 to 16:00, so the installation capacity of the PV system can be increased from 1.949 MW in Case 2.1 to 2.287 MW. However, the addition of the electrical energy storage equipment has no effect on the thermal balance of the system, so the amount of solar thermal accommodation is the same as that in Case 2.1. The electrical and thermal power output of Case 2.3 is shown in Figure 8.
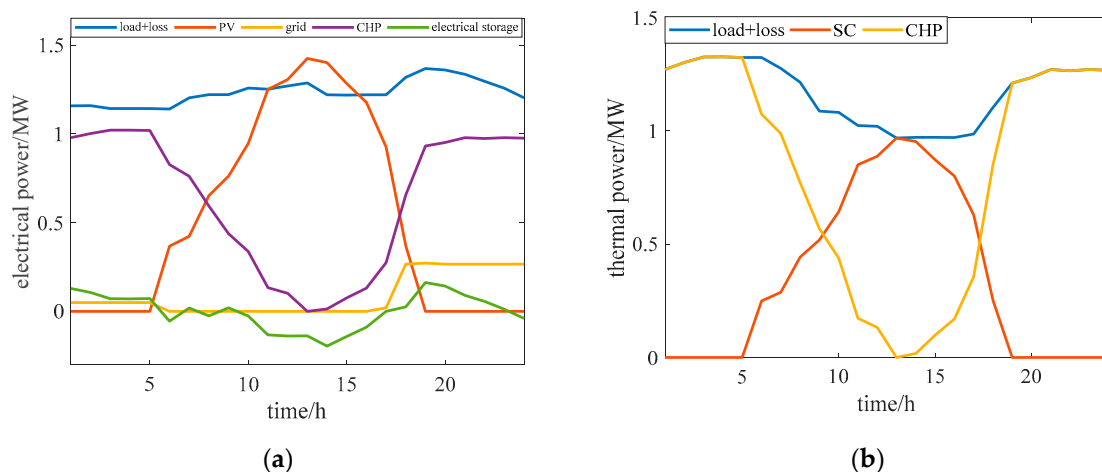
Figure 8. (**a**) Electrical power output in Case 2.3; (**b**) thermal power output in Case 2.3.

(4) In Case 2.4, the installed TES equipment can store heat from 11:00 to 16:00, so the installation capacity of the SC system can be increased from 1.536 MW in Case 2.1 to 1.992 MW. At the same time, due to the installation of heat storage equipment, the CHP unit is maintained at a zero output state during the period from 11:00 to 16:00, which increases the PV installation capacity from 1.949 MW in Case 2.1 to 1.991 MW, with an increase of 0.042 MW. The electrical and thermal power output of Case 2.4 is shown in Figure 9.
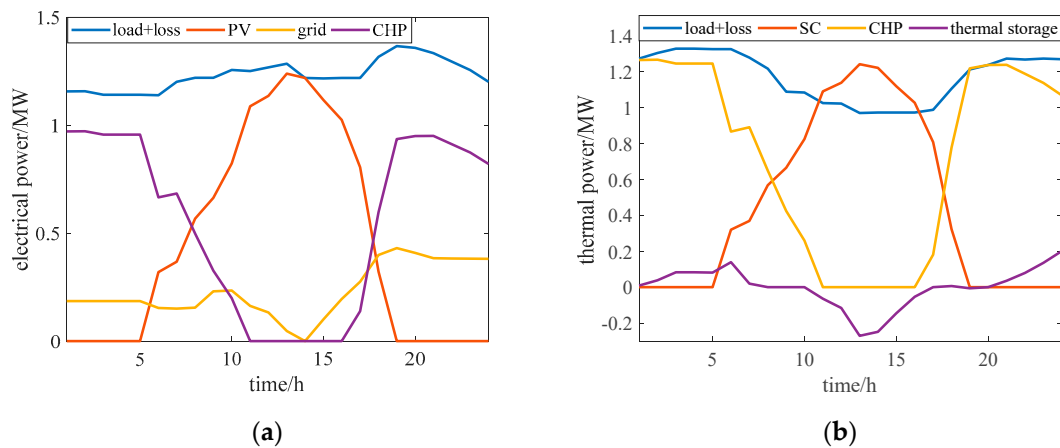
Figure 9. (**a**) Electrical power output in Case 2.4; (**b**) thermal power output in Case 2.4.

(5) In Case 2.5, the system has both heat storage equipment and electrical energy storage equipment installed, and the PV and SC installation capacity of the system increases correspondingly. The PV installation capacity increases from 1.949 MW in Case 2.1 to 2.439 MW. The SC installation capacity can be increased from 1.526 MW in Case 2.1 to 1.992 MW. The overall effect is a sum of the effects of the electrical and thermal energy storage equipment. The electrical and thermal power output of Case 2.5 is shown in Figure 10.
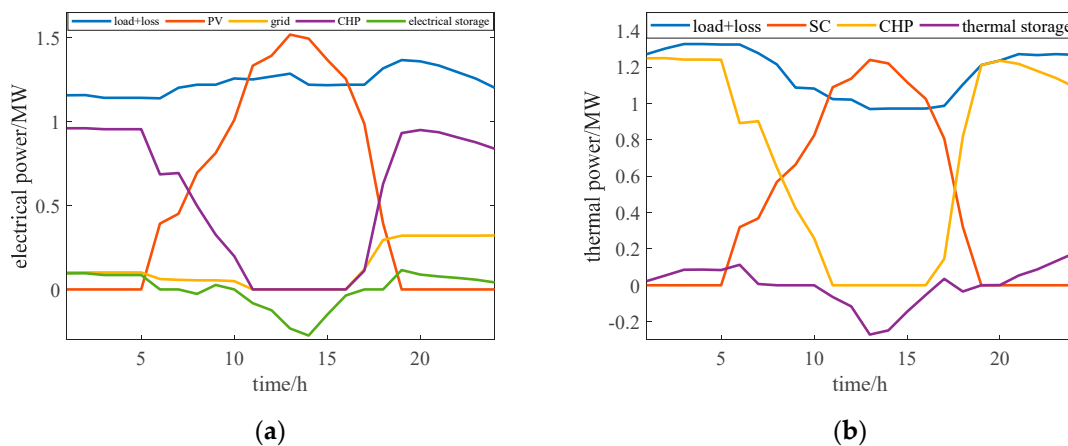
Figure 10. (**a**) Electrical power output in Case 2.5; (**b**) thermal power output in Case 2.5.

In summary, since the GB can only output thermal energy, it has no effect on solar thermal accommodation. However, it can provide more space for solar electricity accommodation by reducing the output of the CHP unit. The electrical energy storage equipment and the TES equipment increase the electrical and thermal loads of the system through the energy storage, so the function of increasing the solar electricity and thermal energy accommodation of the system is obviously improved. In particular, the thermal storage equipment can overcome the electrical-thermal coupling effect of the CHP unit, so the solar electricity accommodation will also exhibit a significant improvement.

The planning capacity of the PVs and SC for each energy station is shown in Figure 11:
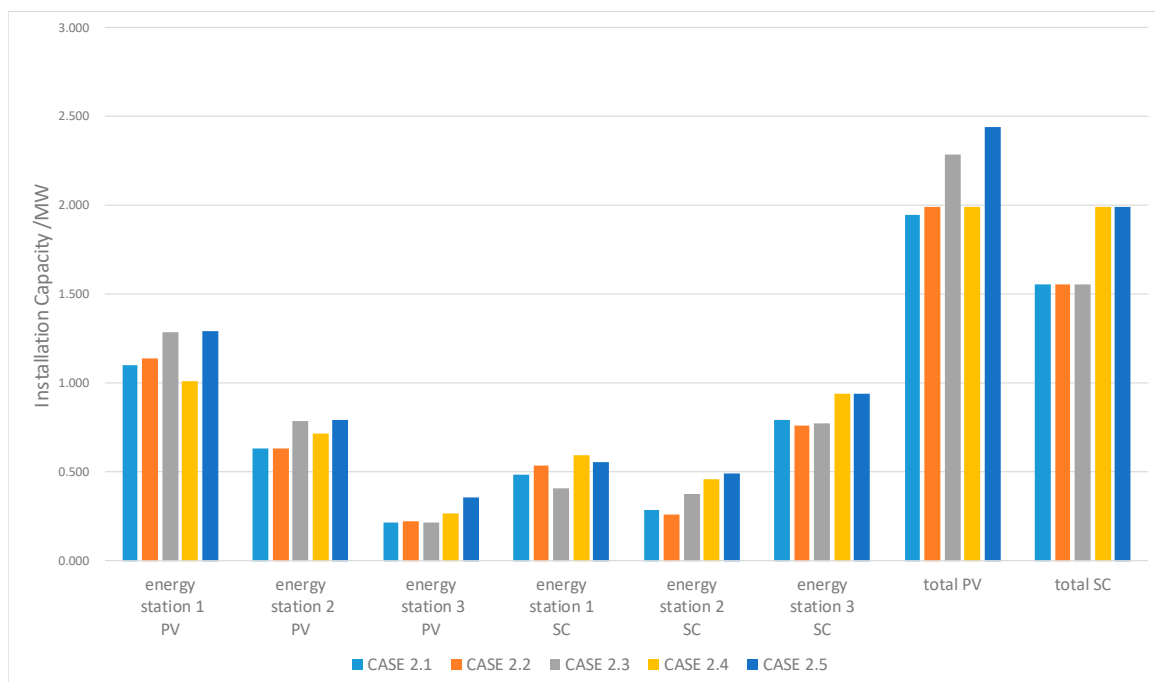
Figure 11. Results of the 24-h period cases.

In each case, the PV and SC installation capacities at each energy station do not increase in proportion. For example, in Case 2.3, the newly added PVs are mainly distributed in energy stations 1 and 2, and the installation capacity of energy station 3 does not increase significantly. This result is mainly due to network loss, and the network loss is smaller in the existing configuration.

5.2.2. Analysis of the Impact of Different Uncertainty Budgets

On the basis of Case 2.5, different values of the uncertainty budget are set, and their effects on the final results are analyzed. Considering that the irradiance intensity curve selected in this paper has 13 h of sunshine, the maximum uncertainty budget is 13.

After calculation and analysis, the results for different uncertainty budgets are shown in Table 3.

Table 3. Analysis of the results for different uncertainty budgets.

Uncertainty Budget	PV Capacity/MW	SC Capacity/MW
1	2.481	2.038
2	2.481	2.038
3	2.481	2.038
4	2.481	2.038
5	2.452	2.010
6	2.439	1.992
7	2.439	1.992
8	2.439	1.992
9	2.439	1.992
10	2.439	1.992
11	2.439	1.992
12	2.439	1.992
13	2.439	1.992

The calculation results in Table 3 show that as the uncertainty budget increases, the PV and SC installation capacity does not gradually decrease; instead, a mutation occurs at the uncertainty values of 5 and 6.

According to the analysis, the two main constraints exist on the maximum PV and SC installation capacity. One is that the PV and SC output cannot exceed the sum of the load and maximum storage capacity of the energy storage equipment. The other is that during the period of high irradiance intensity, the total energy generation exceeding the load should be less than the maximum storage capacity of the energy storage equipment. At the same time, considering the irradiance uncertainty, the maximum PV and SC installation capacity is limited to a few time periods near noon. As the uncertainty budget increases, the effective constraints, that limit the maximum PV and SC installation capacity, change. Figure 12 shows the process of the C&CG algorithm searching for the worst irradiance scenario as the uncertainty increases. When the uncertainty budget is 1, the algorithm adds the upper bounds of the irradiance intensity at 13:00 and 14:00 to the robust optimization constraints, which indicates that these two moments are the most influential moments for solar energy accommodation. When the uncertainty budget increases to 4, 12:00–15:00 is the most influential period. Thus far, the main constraint that restricts solar energy accommodation is the loads and the maximum charge and discharge power of the energy storage equipment. When the uncertainty budget is equal to 5 and 6, the time period affecting solar energy consumption is 11:00–15:00 and 11:00–16:00, where the main constraint changes into the maximum storage capacity of the energy storage equipment during the period. When the uncertainty budget is greater than 6, the solar energy accommodation does not change any further, indicating that the irradiance intensity fluctuations in other periods are not effective constraints for solar energy accommodation. In addition, as shown in the figure, the C&CG algorithm can find effective constraints that degrade the objective function value, but lead to a faster convergence characteristic, with convergence usually occurring after 2 to 4 iterations. The period within the dotted line in Figure 12 is the period of active constraints.
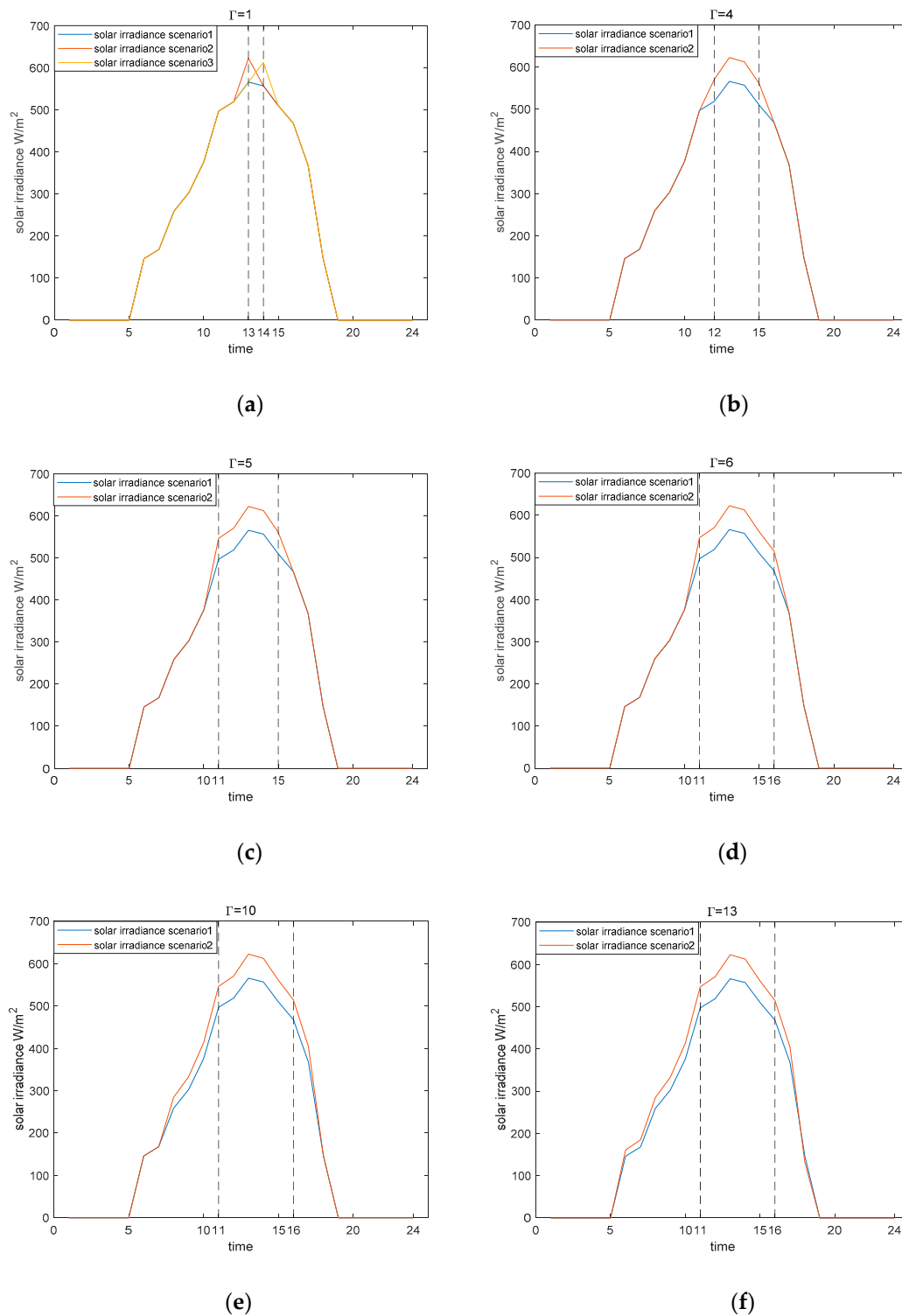
Figure 12. The iterative process of the algorithm for different uncertainty budgets. (**a**) iterative process when Γ = 1; (**b**) iterative process when Γ = 4; (**c**) iterative process when Γ = 5; (**d**) iterative process when Γ = 6; (**e**) iterative process when Γ = 10; (**f**) iterative process when Γ = 13.

6. Discussion

The robust assessment model proposed in this paper can be used to determine the maximum accommodation of solar energy securely in IEs and the corresponding configuration of solar energy equipment. The solar energy accommodation capability increases with both PVs and SCs compared

with PVs only, which is verified in the case study. Except for PVs and SCs, the model proposed can also be applied with other solar energy equipment. The assessment result is helpful to enlarge the utilization of solar energy of IEs. In order to deal with the influence of uncertainty of solar irradiance on the system, the model proposed is based on robust optimization theory. Compared with the deterministic and stochastic model proposed in Reference [11–13], the assessment model proposed in this paper can better ensure the security of the system. The solar energy accommodation capability decreases with the irradiation fluctuation ranges increasing for security. Identifying the reasonable irradiation fluctuation range is a key factor in the robust assessment. History data analysis is a recommended way to structure the fluctuation range. In addition, the assessment result can also evaluate the promotion of different energy equipment, such as gas boilers, and energy storage. This can be used to determine the reasonable configuration of other energy equipment and realize the maximum utilization of solar energy.

7. Conclusions

In this paper, a robust assessment model of solar energy accommodation in district IESs is proposed. The influence of irradiance fluctuation range and some energy equipment is analyzed in different scenarios. When comparisons are made between different scenarios, the following conclusions are drawn:

(1) Compared with the solar energy accommodation in the form of electricity, the electrical-thermal energy comprehensive utilization increases, not only solar energy accommodation in the form of heat directly, but also more PV power by providing more accommodation space and reducing the CHP unit's output. As exemplified in the case study, the system accommodates more PV power of 1.068 MW with growth rate of 60%, and accommodates more 3.172 MW of solar thermal power. Meanwhile, with the solar irradiance fluctuation range increasing from 5% to 20 %, the total solar energy accommodation decreases from 6.25 to 5.73 MW. That means the proposed robust model could provide more secure accommodation capacity indictor and corresponding configuration, with reasonable irradiation fluctuation range prediction.

(2) Gas boiler and energy storage equipment can significantly improve the solar electrical and thermal accommodation capability. The improvement effect varies with different equipment. The electrical accommodation capability increases from 1.949 MW in Case 2.1 to 1.991 MW with a GB of 0.2 MW. While the electrical accommodation capability increases from 1.949 MW to 1.991 MW with electrical energy storage equipment of 0.3 MW and 0.9 MWh. With electrical and thermal energy storage equipment of 0.3 MW and 0.9 MWh, the thermal accommodation capability increases from 1.536 MW to 1.992 MW and the electrical accommodation capability increases from 1.949 MW in Case 2.1 to 1.991 MW. Thus, the reasonable energy equipment configuration could be identified with the proposed model.

(3) In the limited allowable area, there is a certain competitive relationship between PV and SC equipment. As the fluctuation of irradiance increases slightly, the installation capacity of SC increases, while the capacity of PV decreases. When the uncertainty increases further, it may lead the allowable area constraints out of work. The capacity of PV and SC will both decrease.

(4) Not all constraints are effective constraints to solar energy accommodation. With the increase in uncertainty, the effective constraints will change. Through the analysis of uncertainty budget, the critical time which restricts the solar energy accommodation could be found so that more targeted solutions can be made accordingly.

The proposed model fully considers the fluctuation of illumination intensity and the constraints of electric and thermal networks, and can reasonably evaluate the maximum solar energy accommodation capacity of district integrated energy system. This paper does not consider the effect of appropriate solar energy curtailment on the overall accommodation capability of solar energy. In future studies, the cost of equipment installation will be looked at. The influence of different types of thermal-electrical coupling devices on solar energy accommodation could also be further studied.

Conflicts of Interest: The authors declare no conflict of interest.

Nomenclature

Acronyms

IES	Integrated energy system
CHP	Combined heat and power
TES	Thermal energy storage
HP	Heat pump
PV	Photovoltaic
SC	Solar collector

Subscripts and superscripts

pv	Photovoltaic
col	Solar collector
chp	Combined heat and power
gb	Gas boiler
es	Electrical energy storage
ts	Thermal energy storage

Variables

$P_{i,pv}$	Actual output power of the PV at node i
$P_{i,chp}$	Power output of the CHP unit at node i
$P_{es,i,t}$	Charging and discharging power at time t
$P_{dis}^{\max}$	Maximum discharging power of electrical storage device
$P_{cha}^{\max}$	Maximum charging power of electrical storage device
P_i	Active injected power of node i
P_{grid}	Active power injected by large power grid
$P_{i,load}$	Active load at node i
P_{ij}	Active power from node i to node j
P_{loss}	Total power grid loss
Q_i	Reactive injected power of node i
Q_{grid}	Reactive power injected by large power grid
$Q_{i,load}$	Reactive load at node i
Q_{ij}	Reactive power from node i to node j
U_i	Voltage amplitude of node i
$\underline{U}$	Upper limits of the node voltage
$\overline{\overline{U}}$	Lower limits of the node voltage
I_{ij}	Current amplitude of branch ij
$\overline{I}$	Maximum allowable current of the branch
r_{ij}	Resistance of branch ij
x_{ij}	Reactance of branch ij
$H_{i,col}$	Thermal output of the SC at node i
$H_{i,chp}$	Thermal output of the CHP unit at node i
$H_{i,gb}$	Thermal output of the gas boiler at node i
$\overline{H}_{i,gb}$	Maximum thermal output of gas boiler at node i
$H_{ts,i,t}$	Charging and discharging heat at time t
$H_{dis}^{\max}$	Maximum discharging heat of thermal storage device
$H_{cha}^{\max}$	Maximum charging heat of thermal storage device

$H_{s,i}$	Thermal power injected into node i
H'_{ij}	Available thermal power contained in the thermal medium flowing into node i of the water supply pipe ij
$\Delta H'$	Loss of thermal power in the pipe
$H'^{\min}_{ij}$	Minimum thermal power transmitted in the pipe ij
$H'^{\max}_{ij}$	Maximum thermal power transmitted in the pipe ij
$\sum R$	Thermal resistance of the pipe per kilometer
$v^{\max}_{ij}$	Maximum allowable velocity in the pipe ij
S_{ij}	Cross-sectional area of the pipe ij
T_s	Water supply temperature
T_r	Water return temperature
T_a	Environment temperature
l_{ij}	Length of the pipeline
c_p	Specific heat capacity of the fluid
ρ	Fluid density
$A_{i,pv}$	Installation area of the PV system at node i
$A_{i,col}$	Installation area of the SC at node i
$\overline{A_i}$	Maximum area of solar energy equipment installed at node i
I_i	Actual solar irradiance at node i
I_S	Solar irradiance under standard conditions
$\widetilde{I}$	Actual solar irradiance
$\hat{I}$	Predicted solar irradiance
ΔI	Fluctuation range of solar irradiance set according to the actual situation
U	Uncertainty set
Γ	Uncertainty adjustment budget
η_{pv}	PV conversion efficiency of the PV system
η_{col}	Efficiency of the SC
$C_{i,pv}$	PV capacity installed at node i
$C_{i,col}$	SC capacity installed at node i
$S_{i,t}$	Storage states of electrical storage devices
$TS_{i,t}$	Storage states of thermal storage devices
$\delta(j)$	Set of head nodes of branches ended with node j
$\xi(j)$	Set of end nodes of the branches whose head node is j
ω	Weight coefficient of power grid loss
τ	Value factor of therm

Appendix A

Table A1. Data of thermal load at each node.

Node Number	Thermal Load (MW)	Node Number	Thermal Load (MW)	Node Number	Thermal Load (MW)	Node Number	Thermal Load (MW)
1	0	9	0.107	17	0.0805	25	0
2	0	10	0.107	18	0.0805	26	0.107
3	0.107	11	0.145	19	0	27	0.107
4	0.145	12	0.107	20	0.0805	28	0
5	0	13	0	21	0.0805	29	0.107
6	0.107	14	0.0805	22	0	30	0.107
7	0.107	15	0	23	0.107	31	0
8	0.107	16	0.0805	24	0.107	32	0

Table A2. Active power of electrical load at each node.

Node Number	Active Power of Electrical Load (MW)
1	0
2	0
3	0.2
4	0.5
5	0.5
6	0
7	0.2
8	0.2
9	0

Table A3. Power system parameters of the system.

Branch No	From Node	To Node	Length (m)	Impedance (Ω/km)
1	1	2	260	$0.164 + j0.080$
2	2	3	170	$0.164 + j0.080$
3	3	4	230	$0.164 + j0.080$
4	4	8	320	$0.164 + j0.080$
5	8	5	200	$0.164 + j0.080$
6	5	6	160	$0.164 + j0.080$
7	6	7	260	$0.164 + j0.080$

Table A4. Thermal system parameters of the system.

Pipe No	From Node	To Node	Length (m)	Diameter (mm)
1	1	2	257.6	125
2	2	3	97.5	40
3	2	4	51	40
4	2	5	59.5	100
5	5	6	271.3	32
6	5	7	235.4	65
7	7	8	177.3	40
8	7	9	102.8	40
9	7	10	247.7	40
10	5	11	160.8	100
11	11	12	129.1	40
12	11	13	186.1	100
13	13	14	136.2	80
14	14	15	41.8	50
15	15	16	116.8	32
16	15	17	136.4	32
17	14	18	136.4	32
18	14	19	44.9	80
19	19	20	136.4	32
20	19	21	134.1	32
21	19	22	41.7	65
22	22	23	161.1	32
23	22	24	134.2	32
24	22	25	52.1	65
25	25	26	136	32
26	25	27	123.3	32
27	25	28	61.8	40
28	28	29	95.2	32
29	28	30	105.1	32
30	31	28	70.6	125
31	31	7	261.8	125
32	32	11	201.3	125

References

1. Yang, J.; Zhang, N.; Wang, Y.; Kang, C. Multi-energy system towards renewable energy accommodation: Review and prospect. *Autom. Electr. Power Syst.* **2018**, *4*, 11–24.
2. Wei, W.; Wang, K.; Li, G.; Fan, L.; Wang, Y. Robust unit commitment to improve the admissible region of wind power. *Trans. China Electrotech. Soc.* **2018**, *33*, 523–532.
3. Lyu, Q.; Jiang, H.; Chen, T.; Wang, H.; Lyu, Y.; Li, W. Wind power accommodation by combined heat and power plant with electric boiler and its national economic evaluation. *Autom. Electr. Power Syst.* **2014**, *38*, 6–12.
4. Hedegaard, K.; Mathiesen, B.V.; Lund, H.; Heiselberg, P. Wind power integration using individual heat pumps—Analysis of different heat storage options. *Energy* **2012**, *47*, 284–293. [CrossRef]
5. Østergaard, P.A. Wind power integration in Aalborg Municipality using compression heat pumps and geothermal absorption heat pumps. *Energy* **2013**, *49*, 502–508. [CrossRef]
6. Chen, L.; Xu, F.; Wang, X.; Min, Y.; Ding, M.; Huang, P. Implementation and effects of thermal storage in improving wind power accommodation. *Proc. CSEE* **2015**, *35*, 4283–4290.
7. Gu, Z.; Kang, C.; Chen, X.; Bai, J.; Cheng, L. Operation optimization of integrated power and heat energy systems and the benefit on wind power accommodation considering heating network constraints. *Proc. CSEE* **2015**, *35*, 3596–3604.
8. Chen, X.; Lu, X.; Mcelroy, M.B.; Nielsen, C.P.; Kang, C. Synergies of wind power and electrified space heating: case study for Beijing. *Environ. Sci. Technol.* **2014**, *48*, 2016–2024. [CrossRef]
9. Patteeuw, D.; Bruninx, K.; Arteconi, A.; Delarue, E.; D'Haeseleer, W.; Helsen, L. Integrated modeling of active demand response with electric heating systems coupled to thermal energy storage systems. *Appl. Energy* **2015**, *151*, 306–319. [CrossRef]
10. Tang, B.; Gao, G.; Xia, X.; Yang, X. Integrated energy system configuration optimization for multi-zone heat-supply network interaction. *Energies* **2018**, *11*, 3052. [CrossRef]
11. Huang, R.; Pu, T.; Liu, K.; Yang, Z.; Chen, N. Photovoltaic accommodation capacity determination of actual feeder based on stochastic scenarios analysis with storage system considered. *Autom. Electr. Power Syst.* **2015**, *39*, 34–40.
12. Jia, W.; Kang, C.; Dan, L.I.; Chen, Z.; Liu, J. Evaluation on capability of wind power accommodation based on its day-ahead forecasting. *Power Syst. Technol.* **2012**, *36*, 69–75.
13. Wang, X.; Qiao, Y.; Lu, Z.; Ding, L.; Shao, G.; Xu, X.; Hou, K. A novel method to assess wind energy usage in the heat-supplied season. *Proc. CSEE* **2015**, *35*, 2112–2119.
14. Wang, H.; Yin, W.; Abdollahi, E.; Lahdelma, R.; Jiao, W. Modelling and optimization of CHP based district heating system with renewable energy production and energy storage. *Appl. Energy* **2015**, *159*, 401–421. [CrossRef]
15. Perea-Moreno, A.J.; Miguel-Ángel, P.M.; Hernandez-Escobedo, Q.; Manzano-Agugliaro, F. Towards forest sustainability in Mediterranean countries using biomass as fuel for heating. *J. Clean. Prod.* **2017**, *156*, 624–634. [CrossRef]
16. Perez-Mora, N.; Bava, F.; Andersen, M.; Bales, C.; Lennermo, G.; Nielsen, C.; Furbo, S.; Martínez-Moll, V. Solar district heating and cooling: A review. *Int. J. Energy Res.* **2017**, *42*, 1419–1441. [CrossRef]
17. Böttger, D.; Götz, M.; Lehr, N.; Kondziella, H.; Bruckner, T. Potential of the power-to-heat technology in district heating grids in Germany. *Energy Procedia* **2014**, *46*, 246–253. [CrossRef]
18. Xu, C.; Liu, T.; Sui, J.; Liu, Q. Evaluation method for energy saving ratio of distributed energy system with multi-energy thermal complementarity. *Autom. Electr. Power Syst.* **2018**, *42*, 151–157.
19. Rosen, M.A.; Le, M.N.; Dincer, I. Efficiency analysis of a cogeneration and district energy system. *Appl. Therm. Eng.* **2005**, *25*, 147–159. [CrossRef]
20. Rezaie, B.; Reddy, B.V.; Rosen, M.A. Exergy analysis of thermal energy storage in a district energy application. *Renew. Energy* **2015**, *74*, 848–854. [CrossRef]
21. Ibrahim, D. The role of exergy in energy policy making. *Energy Policy* **2002**, *30*, 137–149.
22. Aien, M.; Hajebrahimi, A.; Fotuhi-Firuzabad, M. A comprehensive review on uncertainty modeling techniques in power system studies. *Renew. Sustain. Energy Rev.* **2016**, *57*, 1077–1089. [CrossRef]
23. Correa-Florez, C.A.; Gerossier, A.; Michiorri, A.; Kariniotakis, G. Stochastic operation of home energy management systems including battery cycling. *Appl. Energy* **2018**, *225*, 1205–1218. [CrossRef]

24. Kamjoo, A.; Maheri, A.; Dizqah, A.M.; Putrus, G.A. Multi-objective design under uncertainties of hybrid renewable energy system using NSGA-II and chance constrained programming. *Int. J. Electr. Power Energy Syst.* **2016**, *74*, 187–194. [CrossRef]

25. Guo, Y.; Zhao, C. Islanding-aware robust energy management for microgrids. *IEEE Trans. Smart Grid* **2016**, *9*, 1301–1309. [CrossRef]

26. Jabr, R.A. Radial distribution load flow using conic programming. *IEEE Trans. Power Syst.* **2006**, *21*, 1458–1459. [CrossRef]

27. Tao, D.; Liu, S.; Wei, Y.; Bie, Z.; Bo, Z. A Two-stage robust reactive power optimization considering uncertain wind power integration in active distribution networks. *IEEE Trans. Sustain. Energy* **2015**, *7*, 301–311.

28. Gilbert, G.M.; Bouchard, D.E.; Chikhani, A.Y. A comparison of load flow analysis using DistFlow, Gauss-Seidel, and optimal load flow algorithms. In Proceedings of the IEEE Canadian Conference on Electrical and Computer Engineering, Waterloo, ON, Canada, 25–28 May 1998; Volume 852, pp. 850–853.

29. Wang, B.; Tang, N.; Zhao, S.; Lin, K.; Wang, Y.; Xiao, Y. Stochastic & adjustable robust hybrid scheduling model of power system considering demand response's participation in large-scale wind power consumption. *Proc. CSEE* **2017**, *37*, 6339–6346.

30. Farivar, M.; Low, S.H. Branch flow model: Relaxations and convexification—Part I. *IEEE Trans. Power Syst.* **2013**, *28*, 2554–2564. [CrossRef]

31. Wei, G.; Shuai, L.; Wang, J.; Yin, X.; Zhang, C.; Wang, Z. Modeling of the heating network for multi-district integrated energy system and its operation optimization. *Proc. CSEE* **2017**, *37*, 1305–1315.

32. Bo, Z.; Long, Z. Solving two-stage robust optimization problems using a column-and-constraint generation method. *Oper. Res. Lett.* **2013**, *41*, 457–461.

33. Wen, J.; Zeng, B.; Zhang, J. Adjustable robust optimization for distributed wind power planning in distribution network. *Power Syst. Technol.* **2016**, *40*, 227–233.

34. Liu, X.; Jenkins, N.; Wu, J.; Bagdanavicius, A. Combined analysis of electricity and heat networks. *Appl. Energy* **2015**, *162*, 1238–1250.

35. Liu, X.; Wu, H. A control strategy and operation optimization of combined cooling heating and power system considering solar comprehensive utilization. *Autom. Electr. Power Syst.* **2015**, *39*, 1–6.

36. Yang, Y.; Kai, W.; Long, H.; Gao, J.; Xu, Y.; Kato, T.; Suzuoki, Y. Integrated electricity and heating demand-side management for wind power integration in China. *Energy* **2014**, *78*, 235–246. [CrossRef]